Infectivity and antigenicity of SARS-CoV-2 B.1.617 variants

Youchun Wang (wangyc@nifdc.org.cn)
National Institutes for Food and Drug Control https://orcid.org/0000-0001-9769-5141

Li Zhang
National Institutes for Food and Drug Control

Qianqian Li
National Institutes for Food and Drug Control

Jiajing Wu
National Institutes for Food and Drug Control

Yuanling Yu
National Institutes for Food and Drug Control

Yue Zhang
National Institutes for Food and Drug Control

Jianhui Nie
National Institutes for Food and Drug Control

Ziteng Liang
National Institutes for Food and Drug Control

Zhimin Cui
National Institutes for Food and Drug Control

Shuo Liu
National Institutes for Food and Drug Control

Jiajing Wu
National Institutes for Food and Drug Control

Ruxia Ding
National Institutes for Food and Drug Control

Fei Jiang
National Institutes for Food and Drug Control

Tao Li
National Institutes for Food and Drug Control

Lingling Nie
National Institutes for Food and Drug Control

Qiong Lu
National Institutes for Food and Drug Control

Jiayi Li

National Institutes for Food and Drug Control

Lili Qin

Acro Biosystems, Inc.

Yinan Jiang

Acro Biosystems, Inc.

Yi Shi

Institute of Microbiology, Chinese Academy of Sciences

Wenbo Xu

MHC Key Laboratory of Biosafety, National Institute for Viral Disease Control and Prevention, China CDC

Weijin Huang

National Institutes for Food and Drug Control (NIFDC) https://orcid.org/0000-0002-4246-8889

Biological Sciences - Article

Keywords:

Posted Date: June 10th, 2021

DOI: https://doi.org/10.21203/rs.3.rs-596463/v1

Infectivity and antigenicity of SARS-CoV-2 B.1.617 variants

Li Zhang[1,6], Qianqian Li[1,2,6], Jiajing Wu[1,6], Yuanling Yu[1,6], Yue Zhang[1,6], Jianhui Nie[1,6], Ziteng Liang[1], Zhimin Cui[1], Shuo Liu[1], Haixin Wang[1], Ruxia Ding[1], Fei Jiang[1], Tao Li[1], Lingling Nie[1], Qiong Lu[1], Jiayi Li[1], Lili Qin[5], Yinan Jiang[5], Yi Shi[3*], Wenbo Xu[4*], Weijin Huang[1*], and Youchun Wang[1,2,7*]

[1]Division of HIV/AIDS and Sex-transmitted Virus Vaccines, Institute for Biological Product Control, National Institutes for Food and Drug Control (NIFDC) and WHO Collaborating Center for Standardization and Evaluation of Biologicals, No. 31 Huatuo Street, Daxing District, Beijing 102629, China.

[2]Graduate School of Peking Union Medical College, No. 9 Dongdan Santiao, Dongcheng District, Beijing 100730, China

[3]CAS Key Laboratory of Pathogenic Microbiology and Immunology, Institute of Microbiology, Chinese Academy of Sciences, Beijing 100101, China; Research Network of Immunity and Health (RNIH), Beijing Institutes of Life Science, Chinese Academy of Sciences, Beijing 100101, China.

[4]National Institute for Viral Disease Control and Prevention, Chinese Center for Disease Control and Prevention, Beijing 102206, China

[5]Acro Biosystems, Inc., 8 N. Hongda Rd., Beijing Economic-Technological Development Area, Beijing 100176, China

[6]These authors contributed equally to this work.

[7]Lead contact

*Correspondence: shiyi56@126.com (Y.S.), xuwb@ivdc.chinacdc.cn (W.X.), huangweijin@nifdc.org.cn (W.H.), or wangyc@nifdc.org.cn (Y.W.)

Abstract

SARS-CoV-2 has caused the COVID-19 pandemic. Recently, B.1.617 variants have been transmitted rapidly in India. The transmissibility, pathogenicity, and neutralization characteristics of these variants have received considerable interest. In this study, 22 pseudotyped viruses were constructed for B.1.617 variants and their corresponding single amino acid mutations. B.1.617 variants did not exhibit significant enhanced infectivity in human cells, but mutations T478K and E484Q in the receptor binding domain led to enhanced infectivity in mouse ACE2-overexpressing cells. Furin activities were slightly increased against B.1.617 variants and cell–cell fusion after infection of B.1.617 variants was enhanced. Furthermore, B.1.617 variants escaped neutralization by several mAbs, mainly because of mutations L452R, T478K, and E484Q in the receptor binding domain. The neutralization activities of sera from convalescent patients, inactivated vaccine-immunized volunteers, adenovirus vaccine-immunized volunteers, and SARS-CoV-2 immunized animals against pseudotyped B.1.617 variants were reduced by approximately twofold, compared with the D614G variant.

Main

As of 28 May 2021, there were more than 168 million confirmed cases of COVID-19 worldwide, with a death total exceeding 3 million (https://covid19.who.int). Although several vaccines have been approved and numerous people have been vaccinated in many countries, the pandemic has not yet been effectively controlled. New local COVID-19 outbreaks are always accompanied by the emergence of new SARS-CoV-2 variants[1].

Since March 2021, there has been an outbreak of COVID-19 in India[2]. Viruses of the B.1.617 lineage have been identified as the main SARS-CoV-2 variants related to the outbreak of COVID-19 in India[2]. The B.1.617 variant was first discovered in India on October 2, 2020. Thus far, three sub-lineages B.1.617.1, B.1.617.2, and B.1.617.3 have been derived from the B.1.617 root lineage. Mutation sites involved in these sub-lineages include T19R, T95I, G142D, E154K, F157del, R158del, L452R, T478K, E484Q, D614G, P681R, D950N, Q1071H, and H1101D. Three common mutations (L452R, D614G, and P681R) are shared by all viruses of the B.1.617 lineage. Additionally, two mutations exist in the receptor-binding domain (RBD) of the SARS-CoV-2 spike protein which are L452R and E484Q in B.1.617.1 and 3 or L452R and T478K in B.1.617.2[3].

The major mutation sites of B.1.617 (e.g., L452R, E484Q, D614G, and P681R) are identical or similar to those in other globally circulating SARS-CoV-2 variants. Among them, L452R is the representative mutation site of variants B.1.427 and B.1.429[4]. This mutation enhances binding with ACE2, increases viral infectivity, and reduces neutralization sensitivity[4,5]. The E484Q mutation site in B.1.617 is similar to mutations in variants B.1.351 and P.1(E484K), which is a key site that lead to immune escape[6-11].The D614G mutation has spread fast and alters SARS-CoV-2 fitness, nearly all SARS-CoV-2 viruses thus far contain the D614G mutation[12-14]. Finally, the P681R mutation locates upstream of the furin restriction site (PRRAR)[15]. A similar mutation, P681H, has been identified in B.1.1.7, which were reported to promote cleavage of the S protein precursor[16] and affect O-glycosylation of the spike protein[17], but may not substantially impact viral entry or cell–cell spread[16].

In this study, we constructed a series of SARS-CoV-2 pseudotyped viruses based on the VSV system. We then systematically analyzed the effects of B.1.617 variants on host tropism, protease hydrolysis, cell–cell fusion ability, and neutralization abilities of monoclonal antibodies, convalescent sera, and SARS-CoV-2 vaccine-immunized sera.

Results

Sequence analysis of B.1.617 variants

According to data from the Outbreak.info project[3], 2981 sequences were classified as B.1.617 lineages as of May 6, 2021. Among them, 1602, 1149 and 69 sequences belonged to the B.1.617.1, B.1.617.2 and B1.617.3 sub-lineage respectively while the remaining unclassified 161 belonged to the B.1.617 root lineage. The proportions of distinct single mutations were compared among lineages. Based on mutation frequency differences, each of three B.1.617 sub-lineages was defined as H for high-frequency variants (comprising mutations with >90% frequency) and L for low-frequency variants (comprising mutations between 30% and 90% frequency) (Fig. 1A). Pseudotyped viruses for all the three sub-lineages with both high- and low-frequent mutations were constructed. Meanwhile, all single point mutations composed the variants, as well as pairwise combinations of mutations in the RBD region, was also constructed. The D614G single point mutation based on the original strain was used as the reference sequence (Fig. 1B).

Infectivity and animal tropism

The infectivities of B.1.617 variants were slightly increased in four SARS-CoV-2 susceptible cell lines: Huh-7, Vero, Calu-3, and LLC-MK2 (less than twofold). Investigation of single mutations indicated that the Q1071H and H1101D single mutations and the combinations of L452R with T478K or E484Q could slightly enhance infectivity (Fig. 2A).

To investigate the host range changes of B.1.617 variants, we tested 14 ACE2-overexpressing 293T cell lines from various species. The results suggested that the RBD-specific mutations L452R, T478K, and E484Q significantly enhanced viral infectivity of mouse ACE2-overexpressing cells, compared with the D614G reference strain. There were no significant differences in viral infectivity for other species among B.1.617 sub-lineages (Fig. 2B and Fig. S1).

Proteolytic enzyme effects

Because all B.1.617 variants carry the P681R mutation, adjacent to the proteolytic site, we investigated the influence of protease overexpression (using multiple proteases) on viral infectivity. The increased infectivities by furin overexpression in B.1.617 variants were slightly greater than that of the D614G reference strain (Fig. 2C). A similar phenomenon was not observed upon TMPRSS2 overexpression.

We subsequently investigated enzyme proteolytic activities by examining the proteolysis of S1 and S2 proteins in pseudotyped virus particles. As shown in Fig. 2D, the S2 proportion was not significantly increased in B.1.617 variants, RBD single mutants, or P681R mutants, compared with the D614G reference strain.

Effects on cell–cell fusion

To examine whether the S proteins of B.1.617 variants and the P681R mutant influenced cell–cell fusion characteristics, a dual reporter system consisting of a pair of split Renilla luciferase (spRL) fused to split green fluorescent protein (spGFP) was used[18]. The strengths of the luciferase or GFP signals indicated the degree of host cell fusion (Fig.2E). The luciferase and fluorescence signals were monitored from 1 to 8 hours after donor and acceptor cells had been mixed. Pseudotyped virus without the classical furin (delta PRRA) site was used as a negative control. The fluorescence signals were 1.2–2.3-fold higher in B.1.617 variant-infected cells than in D614G reference strain (Fig. 2F). The luciferase signals were also compared (Fig. S2), the changes were less obvious than fluorescence signal. Further analyses based on single mutations suggested that the P681R single mutation also enhanced cell–cell spread (Fig. 2F).

Monoclonal antibody neutralization

Monoclonal antibodies (mAbs) against the SARS-CoV-2 spike protein offer promising therapies for COVID-19. We examined the neutralization effect of 16 mAbs, including one mAb in clinical use (CB6)[19] and 17 mAbs currently under investigation. The results suggested that B.1.617.1-H/L and B.1.617.3-H/L variants mainly escaped the X593, 9G11, AbG3, A261-262, and AM180 mAbs. These effects were presumably caused by a L452R and E484Q double mutation in the RBD region. These findings were verified by analyses of pseudotyped viruses with single and combined mutations of L452R and E484Q in the RBD region. B.1.617.2-H/L, which exhibited L452R and T478K mutations in the RBD region, reduced the neutralization effects of

the X593, 9G11, 7B8, AbG3, and AM180 mAbs. Notably, although E484Q and E484K both involve an identical mutation site, E484K allowed escape from the AM128 mAb, whereas E484Q did not. We did not find any impacts of other single point mutations outside the RBD region on the neutralization effects of mAbs (Fig. 3A, see also Figs. S3 and S4).

Structural analysis

We further analyzed the structure of the spike and antibody complex, based on published data. Concerning the X593 mAb, E484 and L452 are located at the RBD–antibody binding interface. Mutation of E484Q creates a charge leads to disruption of the interaction, while mutation of L452R affects the hydrophobic interactions. The mAb 7B8 was the only antibody from which T478K could escape in this study. Mutation of T478K destroys the hydrophobic environment, thus affecting the RBD–antibody interaction. As for mAb 9G11, although L452 and E484 are near the interaction surface, they exhibit minimal interaction forces. The L452R mutation may produce a charge conflict with R64, resulting in reduced affinity. Additionally, the mutations L452R, T478K, and E484Q are far from the binding site with the mAb CB6; thus, they do not directly affect its neutralization interactions (Fig. 3B).

Convalescent sera neutralization

As for patients infected with D614G variant, the B.1.617.1-H/L and B.1.617.3-H/L variants reduced the neutralization activities of convalescent sera by 1.6–2.5-fold, while B.1.617.2-H/L variants reduced the neutralization activities of convalescent sera by 1.2–2.0-fold. Single RBD mutations analysis suggested that L452R or E484Q mutations (including L452R combined with E484Q or T478K mutations) were related to the reduced neutralization effect. Our mutation analysis results also suggested that the E484Q mutation had a greater effect on neutralization than the T478K mutation. Additionally, neutralization against B.1.617-L was more strongly reduced, compared with neutralization against B.1.617-H, suggesting that mutations outside the RBD also affect the neutralization activities of convalescent sera (Fig. 4A).

We also analyzed serum samples from convalescent patients who had been infected with the B.1.1.7 variant. Compared with D614G, the neutralization effects against B.1.617.1-H/L and B.1.617.3-H/L variants were reduced by 1.5–2.3-fold, while the neutralization effects against B.1.617.2-H/L variants were reduced by 1.3–1.4-fold (Fig. 4A).

Vaccine-immunized sera neutralization

The protective abilities of two vaccines that have been approved in China have been tested: an inactivated vaccine[20] and an adenovirus vector vaccine[21]. Compared with the D614G reference strain, the B.1.617.1-H/L, B.1.617.2-H/L, and B.1.617.3-H/L variants reduced the neutralization activities of inactivated vaccine-immunized sera by 1.4–2.1, 1.4–2.3, and 1.6–2.4-fold, respectively; and reduced the neutralization activities of adenovirus vaccine-immunized sera by 1.2–1.7, 0.9–1.4, and 1.4–1.7-fold, respectively. Notably, the low-frequency variants with more mutations consistently reduced the neutralization abilities to a greater extent, compared with the high-frequency variants. Single-mutation analyses indicated that E484Q was the main source of neutralization resistance, whereas the L452R and T478K mutations showed weaker effects. Furthermore, E484Q induced neutralization resistance to an extent comparable with the resistance induced by E484K. Overall, although the B.1.617 variants reduced the neutralization abilities of

various vaccines by approximately 0.9–2.4-fold, suggesting both vaccines continued to exhibit a protective effect (Fig. 4B).

Neutralization of animals immunized sera

We first tested neutralization activities of RBD protein-immunized horse sera. Their neutralization activities were significantly reduced (by 3-4-fold) against all B.1.617 variants, as well as the L452R, T478K, and E484Q single or double mutants. (Fig. 4C). The neutralization activities of sera from animals immunized with other variants (e.g., D614G, B.1.351, and B.1.429) were also tested. Full-length spike DNA plus pseudotyped virus was used to immunize mice, yielding a series of post-immunization sera. Analysis of immunized sera suggested that antisera obtained by immunization with B.1.351 and B.1.429 immunogens showed no decreased neutralization activities against B.1.617 variants, compared with the D614G reference strain (Fig. 4D).

Discussion

In India, the prevalence of B.1.617 sub-lineages has increased in a manner consistent with the surge of COVID-19 cases[2,3]; Among them, B.1.617.1 and B.1.617.2 comprise 21% and 7% of sequences, respectively[3]. Furthermore, the proportion of B.1.617.2 sequences is markedly increasing, whereas the proportion of B.1.617.3 sequences is limited[22]. In a recent WHO weekly epidemiological update (11 May 2021), the B.1.617 variant was identified as the fourth VOC[23].

The B.1.617.1 and B.1.617.2 variants are predicted to have increased transmissibility[24]. Previous studies concern SARS-CoV-2 mutations[25] and a structural analysis of B.1.617 major mutations (L452R, E484Q, and P681R) suggested increased ACE2 binding by these variants[26]. Our results suggested entry abilities into Huh-7, Calu-3, Vero, and LLC-MK2 cell lines were not significantly increased. Notably, similar as K417N, N501Y, and E484K in the B.1.351 variant[8], RBD mutations in the B.1.617 variants also showed enhanced infectivity in mouse cells. The causes of increased affinity for mouse ACE2, as well as the structural differences between mouse and human ACE2 proteins, require further analyses.

The SARS-CoV-2 spike protein is hydrolyzed to S1 and S2, which is the first step of virus infection and the prerequisite for virus–cell fusion[27,28]. B.1.617 variants contain a P681R mutation, which is located adjacent to this cleavage site; structural prediction has suggested that the S1–S2 clearance rate of B.1.617 might be affected. Our results suggested that the B.1.617 variants are slightly more sensitive to furin overexpression. Cell–cell fusion provides an additional route for viral dissemination throughout the host. Because the ability to transmit between cells is particle-independent, immune factors (e.g., antibodies) have been presumed to poorly block this type of spread[29]. By using the dual split reporter system, we found a twofold greater tendency for fusion in B.1.617 variants, compared with the D614G reference strain. The increased furin activity and cell-cell spread may explain the increased transmissibility of B.1.617.

Three RBD mutations L452R, T478K and E484Q in B.1.617 can cause immune escape from multiple mAbs, which should be carefully considered in clinical mAb therapy. Additionally, we compared the E484Q and E484K mutations. While the 9G11, AbG3, and AM128 mAbs were more affected by the E484K mutation, the X593 and AM180 mAbs reacted similarly to viruses

containing either mutation. Moreover, we did not observe considerable synergistic effects between L452R and E484Q or T478K and E484Q. Structural analysis could explain these results: mutations in the B.1.617 variant are precisely at the mAb–spike interface.

Reduced neutralization activities against B.1.617 variants were reported for mRNA-1273 vaccine-elicited sera (3–7 fold)[30], and inactivated vaccine BBV152 (1.84 fold)[31]. We tested two vaccines approved in China: inactivated vaccine (KCONVAC)[20] and adenovirus vaccine (Ad5-nCoV)[21]. The neutralization activities of which reduced approximately twofold. Experiments using pseudoviruses B.1.429 (containing L452R) and B.1.351 (containing E484K) as immunogens in mice revealed that the immune sera did not reduce neutralization activity against the B.1.617 variants, compared with the D614G reference strain, suggesting that key mutation sites (e.g., L452 and E484) shared in B.1.617 and B.1.429 or B.1.351 play an important role in immunogenicity.

When the neutralization sensitivities were compared among B.1.617 variants, the neutralizing antibody titers of low-frequency B.1.617 variants with more mutation sites were always more obviously reduced, compared with the high-frequency B.1.617 variants. As they have identical RBD mutation sites, other non-RBD mutations may be responsible for the further reduction of neutralization activity. These results are in compliance with reports about neutralizing mAbs against NTD[32] and another SARS-CoV-2 receptor AXL that binds to NTD [33].

Finally, recent research by Khoury et al. showed that the level of antibody for neutralization for 50% protection against detectable SARS-CoV-2 infection was 20.2% of the mean convalescent antibody level. To protect against severe disease, 3% of the mean convalescent antibody level is sufficient[34.] Neutralization activities against B.1.617 were reduced by approximately twofold in vaccine-immunized sera, suggesting that the current vaccines remain protective.

References

1 Garcia-Beltran, W. F. *et al*. Multiple SARS-CoV-2 variants escape neutralization by vaccine-induced humoral immunity. *Cell* **184**, 2523, doi:10.1016/j.cell.2021.04.006 (2021).

2 Singh, J., *et al*. SARS-CoV-2 variants of concern are emerging in India. *Nature medicine*, doi:10.1038/s41591-021-01397-4 (2021).

3 Outbreak.info. Julia L. Mullen, Ginger Tsueng, Alaa Abdel Latif, Manar Alkuzweny, Marco Cano, Emily Haag, Jerry Zhou, Mark Zeller, Nate Matteson, Kristian G. Andersen, Chunlei Wu, Andrew I. Su, Karthik Gangavarapu, Laura D. Hughes, and the Center for Viral Systems Biology outbreak.info. Available online: https://outbreak.info/ (2020).

4 Deng, X. *et al*. Transmission, infectivity, and neutralization of a spike L452R SARS-CoV-2 variant. *Cell*, doi:10.1016/j.cell.2021.04.025 (2021).

5 Li, Q. *et al*. The Impact of Mutations in SARS-CoV-2 Spike on Viral Infectivity and Antigenicity. *Cell* **182**, 1284-1294.e1289, doi:10.1016/j.cell.2020.07.012 (2020).

6 Wise, J. Covid-19: The E484K mutation and the risks it poses. *BMJ* **372**, n359, doi:10.1136/bmj.n359 (2021).

7 Wang, P. *et al.* Increased resistance of SARS-CoV-2 variant P.1 to antibody neutralization. *Cell host & microbe* **29**, 747-751.e744, doi:10.1016/j.chom.2021.04.007 (2021).

8 Li, Q. *et al.* SARS-CoV-2 501Y.V2 variants lack higher infectivity but do have immune escape. *Cell* **184**, 2362-2371.e2369, doi:10.1016/j.cell.2021.02.042 (2021).

9 Wang, P. *et al.* Antibody resistance of SARS-CoV-2 variants B.1.351 and B.1.1.7. *Nature* **593**, 130-135, doi:10.1038/s41586-021-03398-2 (2021).

10 Planas, D. *et al.* Sensitivity of infectious SARS-CoV-2 B.1.1.7 and B.1.351 variants to neutralizing antibodies. *Nature medicine* **27**, 917-924, doi:10.1038/s41591-021-01318-5 (2021).

11 Hoffmann, M. *et al.* SARS-CoV-2 variants B.1.351 and P.1 escape from neutralizing antibodies. *Cell* **184**, 2384-2393.e2312, doi:10.1016/j.cell.2021.03.036 (2021).

12 Korber, B. *et al.* Tracking Changes in SARS-CoV-2 Spike: Evidence that D614G Increases Infectivity of the COVID-19 Virus. *Cell* **182**, 812-827.e819, doi:10.1016/j.cell.2020.06.043 (2020).

13 Weissman, D. *et al.* D614G Spike Mutation Increases SARS CoV-2 Susceptibility to Neutralization. *Cell host & microbe* **29**, 23-31.e24, doi:10.1016/j.chom.2020.11.012 (2021).

14 Plante, J. A. *et al.* Spike mutation D614G alters SARS-CoV-2 fitness. *Nature* **592**, 116-121, doi:10.1038/s41586-020-2895-3 (2021).

15 Johnson, B. A. *et al.* Loss of furin cleavage site attenuates SARS-CoV-2 pathogenesis. *Nature* **591**, 293-299, doi:10.1038/s41586-021-03237-4 (2021).

16 Lubinski, B., Tang, T., Daniel, S., Jaimes, J. A. & Whittaker, G. R. Functional evaluation of proteolytic activation for the SARS-CoV-2 variant B.1.1.7: role of the P681H mutation. *bioRxiv*, doi:10.1101/2021.04.06.438731 (2021).

17 Zhang, L. *et al.* Furin cleavage of the SARS-CoV-2 spike is modulated by O-glycosylation. *bioRxiv*, doi:10.1101/2021.02.05.429982 (2021).

18 Kondo, N., Miyauchi, K., Meng, F., Iwamoto, A. & Matsuda, Z. Conformational changes of the HIV-1 envelope protein during membrane fusion are inhibited by the replacement of its membrane-spanning domain. *J Biol Chem* **285**, 14681-14688, doi:10.1074/jbc.M109.067090 (2010).

19 Shi, R. *et al.* A human neutralizing antibody targets the receptor-binding site of SARS-CoV-2. *Nature* **584**, 120-124, doi:10.1038/s41586-020-2381-y (2020).

20 Pan, H. X. *et al.* Immunogenicity and safety of a SARS-CoV-2 inactivated vaccine in healthy adults: randomized, double-blind, and placebo-controlled phase 1 and phase 2 clinical trials. *Chinese medical journal*, doi:10.1097/cm9.0000000000001573 (2021).

21 Wu, S. *et al.* A single dose of an adenovirus-vectored vaccine provides protection against SARS-CoV-2 challenge. *Nature communications* **11**, 4081, doi:10.1038/s41467-020-17972-1 (2020).

22 B.1.617.2 Lineage Report. Alaa Abdel Latif, Julia L. Mullen, Manar Alkuzweny, Ginger Tsueng, Marco Cano, Emily Haag, Jerry Zhou, Mark Zeller, Nate Matteson, Chunlei Wu, Kristian G. Andersen, Andrew I. Su, Karthik Gangavarapu, Laura D. Hughes, and the Center for Viral Systems Biology. outbreak.info, (available at https://outbreak.info/situation-reports?pango=B.1.617.2&loc=IND&loc=GBR&loc=USA&selected=IND). Accessed 18 May 2021.

23 WHO. COVID-19 Weekly Epidemiological Update. *https://covid19.who.int* (9 May 2021).

24 Ranjan, R., Sharma, A. & Verma, M. K. Characterization of the Second Wave of COVID-19 in India. 2021.2004.2017.21255665, doi:10.1101/2021.04.17.21255665 %J medRxiv (2021).

25 Starr, T. N. *et al.* Deep Mutational Scanning of SARS-CoV-2 Receptor Binding Domain Reveals Constraints on Folding and ACE2 Binding. *Cell* **182**, 1295-1310.e1220, doi:10.1016/j.cell.2020.08.012 (2020).

26 Cherian, S. *et al.* Convergent evolution of SARS-CoV-2 spike mutations, L452R, E484Q and P681R, in the second wave of COVID-19 in Maharashtra, India. 2021.2004.2022.440932, doi:10.1101/2021.04.22.440932 %J bioRxiv (2021).

27 Shang, J. *et al.* Cell entry mechanisms of SARS-CoV-2. *Proceedings of the National Academy of Sciences of the United States of America* **117**, 11727-11734, doi:10.1073/pnas.2003138117 (2020).

28 Walls, A. C. *et al.* Structure, Function, and Antigenicity of the SARS-CoV-2 Spike Glycoprotein. *Cell* **181**, 281-292.e286, doi:10.1016/j.cell.2020.02.058 (2020).

29 Xia, S. *et al.* Inhibition of SARS-CoV-2 (previously 2019-nCoV) infection by a highly potent pan-coronavirus fusion inhibitor targeting its spike protein that harbors a high capacity to mediate membrane fusion. *Cell research* **30**, 343-355, doi:10.1038/s41422-020-0305-x (2020).

30 Edara, V.-V. *et al.* Infection and vaccine-induced neutralizing antibody responses to the SARS-CoV-2 B.1.617.1 variant. 2021.2005.2009.443299, doi:10.1101/2021.05.09.443299 %J bioRxiv (2021).

31 Yadav, P. D. *et al.* Neutralization of variant under investigation B.1.617 with sera of BBV152 vaccinees. *Clinical infectious diseases*, doi:10.1093/cid/ciab411 (2021).

32 McCallum, M. *et al.* N-terminal domain antigenic mapping reveals a site of vulnerability for SARS-CoV-2. *bioRxiv*, doi:10.1101/2021.01.14.426475 (2021).

33 Wang, S. *et al.* AXL is a candidate receptor for SARS-CoV-2 that promotes infection of pulmonary and bronchial epithelial cells. *Cell research* **31**, 126-140, doi:10.1038/s41422-020-00460-y (2021).

34 Khoury, D. S. *et al.* Neutralizing antibody levels are highly predictive of immune protection from symptomatic SARS-CoV-2 infection. *Nature medicine*, doi:10.1038/s41591-021-01377-8 (2021).

35 Nie, J. *et al.* Quantification of SARS-CoV-2 neutralizing antibody by a pseudotyped virus-based assay. *Nature protocols* **15**, 3699-3715, doi:10.1038/s41596-020-0394-5 (2020).

36 Zhang, L. *et al.* Cellular tropism and antigenicity of mink-derived SARS-CoV-2 variants. *Signal transduction and targeted therapy* **6**, 196, doi:10.1038/s41392-021-00617-0 (2021).

Figure legends

Figure 1. Analysis of mutations in B.1.617 variants.

A.Mutation sites with frequencies of >30% in at least one B.1.617 sub-lineage were tracked using an outbreak website. The heatmap shows the proportions of sequences with each mutation among all sub-lineage sequences.

B. Diagrammatic sketch of B.1.617 variants that were constructed as pseudotyped viruses and analyzed in this study.

Figure 2. Analysis of B.1.617 infectivity, proteolytic activity, and cell–cell fusion

A. Normalized chemiluminescence signals (in RLUs) of target cells were calculated compared with the D614G reference strain. Data represent the results of four replicate experiments. Dotted lines indicate twofold and fourfold change.

B. Equal amounts of ACE2-overexpression plasmids from different species were transfected into 293T cells. Ratios of infectivity compared with the D614G reference strain were shown. Data representing the results of four replicate experiments are shown in heatmap format. Red represents increased infectivity and blue represents decreased infectivity.

C. Proteolytic enzymes furin and TMPRSS2 were separately overexpressed in 293T-hACE2 cells. Data shown indicate relative infectivity changes because of enzyme overexpression. Relative RLUs were compared with or without the indicated enzyme first, then compared with the D614G reference strain. Results were obtained from four independent experiments. Dashed lines indicate the threshold of fourfold difference.

D. B.1.617 and reference pseudotyped viruses were centrifuged in sucrose buffer, then resuspended in PBS for SDS-PAGE. Western blotting was performed with mouse anti-S2 polyclonal antibodies. VSV-M was used as an internal control. Representative results of three replicate experiments are shown.

E. Diagrammatic sketch of dual reporter cell–cell fusion system. 293T cells were used as donor cells.

F. Time course curve of cell–cell fusion. Fluorescence signals of GFP were normalized to the signal of the D614G reference strain after 1 hour of co-incubation; values shown indicate means ± SEMs. Representative results of three independent experiments are shown.

Figure 3. Neutralization activities and structural analyses of mAbs against B.1.617 variants and single point mutations.

A. Data show the neutralization ID_{50} ratio of each variant, compared with the D614G reference strain. Red represents increased neutralization capacity and blue represents decreased neutralization capacity.

B. Structural modelling of the L452R, T478K, and E484Q mutations, based on 7chh for X593, RBD-7B8 for 7B8, RBD-Ab5 for 9G11, and 7c01 for CB6.

Figure 4. Neutralization activities of convalescent sera and immunized sera.

Normalized ID50 ratios compared to D614G reference strain are shown. Means ± SEMs are shown for each variant. Dashed lines indicate the threshold of fourfold difference. Reduced differences (compared with the D614G reference strain) are labeled at the bottom of each plot. All

experiments were repeated 2–4 times, depending on sample availability. A. Neutralization activities of convalescent sera. B. Neutralization activities of vaccine-immunized sera. C. Neutralization activities of RBD protein-immunized horse sera. D. Neutralization activities of sera from full-length spike DNA-immunized and pseudotyped virus-immunized mice. Immunization procedures are shown in the left panel.

Methods

Plasmids and pseudoviruses

The SARS-CoV-2 spike (GenBank: MN908947) protein expression gene was optimized using a mammalian codon and cloned into the pcDNA3.1 vector between BamHI and XhoI restriction sites. Site-directed mutagenesis was performed as described previously[35]; specific mutation sites and corresponding primers are presented in Supplementary Table. Fourteen ACE2-overexpression genes were optimized using a mammalian codon and cloned into the eukaryotic expression vector pRP[Exp]-EGFP-CMV between BamHI and XhoI restriction sites; the sources of these genes were human (BAB40370.1), mink (QNC68911.1), dog (MT663955), cat (MT663959), pangolin (XP_017505746.1), pig (NP_001116542.1), mouse (ABN80106.1), bat (KC881004.1), cow (NP_001019673.2), rabbit (MT663961), ferret (MT663957), sheep (XP_011961657.1), civet (AY881174.1), and monkey (MT663960)[36]. A FLAG tag (GACTACAAGGACGATGACGATAAG) was added at the 3'-terminal end of each gene. The dual split protein system (GFP_{1-7} RL_N / GFP_{8-11} RL_C) was constructed as described by Kondo et al.[18]. Pseudotyped viruses of SARS-CoV-2 variants and single mutants were constructed in accordance with the methods described in our previous study.

Cells

Five cell lines were used in this study: 293T (American Type Culture Collection, ATCC, CRL-3216), Vero (ATCC, CCL-81), LLC-MK2 (ATCC, CCL-7), Calu-3 (ATCC, HTB-55), and Huh-7 (Japanese Collection of Research Bioresources, Cat0403). The cell line 293T-hACE2 comprised 293T cells stably expressing human ACE2.

Fourteen ACE2 protein expression plasmids and two proteolytic enzyme transient overexpression cell lines were prepared by transfection of 293T cells using Lipofectamine 2000 (Invitrogen). All cells were cultured at 37°C in a 5% CO_2 environment using Dulbecco's modified Eagle medium (DMEM, high glucose; HyClone, Logan, UT) with 100 U/mL of penicillin-streptomycin solution (Gibco, Germany), 20 mM N-2-hydroxyethylpiperazine-N-2-ethane sulfonic acid (HEPES, Gibco) and 10% fetal bovine serum (FBS, Pansera ES, PAN-Biotech, Germany). Trypsin-EDTA (0.25%, Gibco) was used to detach cells for subculture at intervals of 2–3 days.

Monoclonal antibodies

Sixteen anti-SARS-CoV-2 monoclonal antibodies (mAbs) were used in this study. The mAb sources were as follows: CB6 was from Dr. Jinghua Yan[19]; X593 and X604 were from Dr. X. Sunney Xie; SCTA01, H02M027, H014, H00S002 and HHV1 were from Dr. Liangzhi Xie of Sino Biological Company; 9G11, 4E5, and 7B8 were from Dr. Yuelei Shen of Beijing Biocytogen Inc.; AbG3 was from Dr. Zhiqiang He of Fapon Biotech Inc.; A261-262 was from Dr. Linqi Zhang of Tsinghua University; and A001, AM180, and AM128 were from Acro Biosystems Co.

Convalescent sera

Serum samples from SARS-CoV-2 convalescent patients were provided by Dr. Wenbo Xu from the Chinese Center for Disease Control and Prevention. Nine samples were from patients in Beijing who had been infected with the D614G reference strain. They had been diagnosed with

COVID-19 during the period from December 2020 to January 2021; the sera had been collected 14–28 days after discharge. Ten serum samples were from patients in Beijing who had been infected with the B.1.1.7 variant. They had been diagnosed with COVID-19 in January 2021; the sera had been collected 14–28 days after discharge. Written informed consent was obtained from all patients prior to blood collection. The study protocol involving convalescent serum samples was approved by the Ethic Committee of Chinese Center for Disease Control and Prevention

Sera from vaccinated participants

Serum samples were collected from individuals who had been immunized with the inactivated vaccine[20] (KCONVAC, Shenzhen Kangtai Biological Products Co.; Chinese Clinical Trial Registry: ChiCTR2000038804); samples were collected at 14 days after the completion of a standard immunization procedure (doses at 0, 28, and 58 days; 5 μg/dose). Twenty samples were used in this study. Written informed consent was obtained from all volunteers prior to blood collection. The study protocol involving the inactivated vaccine was approved by the Ethic Committee of Jiangsu Provincial Center for Disease Control and Prevention.

Serum samples were collected from individuals who had been immunized with the adenovirus vaccine[21] (Ad5-nCoV, CanSino Biologics Inc. ChiCTR2000031781); samples were collected at 28 days after the completion of a standard immunization procedure (one dose at 0 days; 300 μl/dose). Eighteen samples were used in this study. Written informed consent was obtained from all volunteers prior to blood collection. The study protocol involving the adenovirus vaccine was approved by the Ethics Committee of Jiangsu Provincial Center for Disease Control and Prevention.

Sera from immunized animals

Animals were handled under institutional (NIFDC, Beijing, China) guidelines for laboratory animal care and use, and the Animal Care and Use Committee at the NIFDC approved the animal study protocol.

Mice were immunized with purified SARS-CoV-2 plasmid comprising the D614G reference strain, B.1.351 variant, or B.1.429 variant (50 μg per mouse) at day 0. Pseudotyped viruses of the same SARS-CoV-2 variant in combination with aluminum adjuvant were used for the second and third immunization at days 14 and 28 respectively (6×10^5 $TCID_{50}$ per mouse). Blood samples were collected at 14 days after the third immunization. Serum samples from 10 mice were pooled (two mice per sample).

Horses were immunized using the SARS-CoV-2 RBD protein (original strain WH-1; RBD identical to the D614G reference strain) with Freund's incomplete adjuvant at an initial dose of 3 mg. Ten days later, they were immunized again using 6 mg of RBD protein with Freund's incomplete adjuvant. A third immunization was performed at 10 days after the second immunization, using 12 mg of RBD protein with Freund's incomplete adjuvant. Serum samples from four horses were collected at 7 days after the third immunization.

Infectivity assay

Pseudotyped SARS-CoV-2 variants were serially diluted and mixed with Huh-7 cells or other indicated cells, then incubated at 37°C with 5% CO_2. Twenty-four hours later, chemiluminescence signals were collected by the PerkinElmer Ensight device using Britelite plus reporter gene assay system (PerkinElmer) and displayed as relative luminescence units (RLUs). The detailed methods were described in our previous article[5]. Duplicate wells were established for each group. Each experiment was repeated four times. ACE2 expression levels were verified by FACS (Fig. S5).

Neutralization assay

mAbs and serum samples were pre-diluted to specific initial concentrations. Serially diluted samples were then added to 96-well plates, mixed with pseudotyped virus, and incubated at 37°C for 1 hour. Thereafter, 2×10^4 Huh-7 cells/100 μL were added to each well of the 96-well plate. Cells were then incubated at 37°C with 5% CO_2. Chemiluminescence signals were detected after 24 hours. The ID_{50} (50% inhibitory dilution) was calculated using the Reed–Muench method. The results were recorded as the mean of three replicates.

Proteolytic cleavage analysis

For each SARS-CoV-2 variant, 7 mL of pseudotyped virus were added to 2 mL of 25% sucrose buffer and centrifuged at 10,0000 g for 3 hours. Each pellet of purified pseudotyped virus was then re-suspended in 100 μL PBS. Samples were mixed with loading buffer and heated at 100℃ for 5 minutes; a 30-μL aliquot of each sample was then used for SDS-PAGE and western blotting analysis. The primary antibodies were a homemade mouse anti-S2 antibody against SARS-CoV-2 spike protein and a custom anti-VSV M (KeraFast, EB0011) protein antibody; the secondary antibody was a 1:10000 dilution of HRP-conjugated goat anti-mouse IgG (CWbiotech). Immobilon western chemiluminescent HRP substrate (Millipore) was used to develop the immunoreactive bands. Band intensities were calculated using Alphaview software.

Cell–cell fusion assay

Donor cells were 293T cells that had been transfected with separate plasmids harboring the spike genes of distinct SARS-CoV-2 variants or single mutants and the $GFP_{1\text{-}7}$ RL_N plasmid. Acceptor 293T cells stably expressing human ACE2 were transfected with the $GFP_{8\text{-}11}$ RL_C plasmid. The cells were incubated at 37°C with 5% CO_2 for 24 hours, then detached with trypsin. Spike protein expression levels were verified by FACS (Fig. S6). The donor and acceptor cells were mixed at a 1:1 ratio and seeded in 96-well plates. GFP and Renilla luciferase fluorescence values were monitored at 1 to 8 hours after mixing. The GFP signals were collected using BioTek Cytation 5V. The EnduRen live cell substrate (Promega, E6481, WI) and Ensight device (PerkinElmer) were used for luciferase activity detection.

Structural modelling

The spike protein was modelled based on the following Protein Data Bank coordinate sets: 7chh for X593, RBD-7B8 for 7B8, RBD-Ab5 for 9G11, and 7c01 for CB6; these revealed mutations L452R, T478K, and E484Q, respectively. PyMOL software (PyMOL Molecular Graphics System, Version 2.2.0, Schrödinger, LLC.) was used for visualization.

Statistical analysis

GraphPad Prism 8 was used for plotting. One-way ANOVA and Holm–Sidak multiple comparisons tests were used for statistical analysis. Values are shown as means ± SEMs. Significance thresholds were as follows: * $P<0.05$, ** $P<0.01$, *** $P<0.005$, and **** $P<0.001$.

Acknowledgements

We gratefully acknowledge the authors from the originating laboratories and the submitting laboratories where genetic sequence data were generated and shared via GISAID, enabling this research. We thank Prof. Jinghua Yan from Institute of Microbiology, Chinese Academy of Sciences for mAb CB6; Prof. X. Sunney Xie of Peking University for mAbs X593 and X604; Dr. Liangzhi Xie from Sino Biological Company for SCTA01, H02M027, H00S002, H014 and HHV1 mAbs; Dr. Zhiqiang He from Fapon Biotech Inc. for mAb AbG3; Dr. Linqi Zhang of Tsinghua University for mAb A261-262; and Dr. Yuelei Shen of Beijing Biocytogen Inc. for 9G11, 4E5, and 7B8 mAbs. We thank Dr. Jiankai Liu from Shenzhen Kangtai Biological Products Co., Ltd. and Beijing Minhai Biotechnology Co. for providing inactivated vaccine-immunized sera; we thank Prof. Junqiang Li from the Institute of Biotechnology, Academy of Military Medical Sciences, PLA of China and CanSino Biologics Inc. for providing adenovirus vaccine-immunized sera. This work was supported by the National Key Research and Development Program of China [grant number 2021YFC0863300], General Program of the National Natural Science Foundation of China [grant number 82073621], National Science and Technology Major Projects of Drug Discovery [grant number 2018ZX09101001], National Science and Technology Major Projects of Infectious Disease [grant number 2017ZX10304402], and Bill & Melinda Gates Foundation [Investment ID INV-006379]. We thank Ryan Chastain-Gross, Ph.D., from Liwen Bianji (Edanz) (www.liwenbianji.cn), for editing the English text of a draft of this manuscript.

Author contributions

Y.W., L.Z., J.N., and W.H. conceived, designed, and supervised the experiments; L.Z. and Y.W. wrote the manuscript; Q.L., J.W., Z.C., S.L., H.W., R.D., Z.L., F.J., T.L., L.N., Q.L., J.L., L.Q., and Y.J. performed the experiments for infectivity, host tropism, and neutralization; Y.Y. performed cell fusion experiments; Y.Z. performed proteolysis experiments; Y.S. performed structural analyses; and W.X. provided convalescent sera and clinical data. All authors approved the final manuscript.

Competing interests

All authors declare no competing interests.

Figure S1. Animal tropism of B.1.617. Related to Figure 2.
For each group, RLU values were normalized to the values of the D614G reference strain. Data represent the means ± SEMs of four replicate experiments. Dotted line indicates fourfold change.

Figure S2. Cell–cell fusion (RLU). Related to Figure 2F.
Time course curve of cell–cell fusion. RLU signals of Renilla luciferase were normalized to the signal of the D614G reference strain after 1 hour of co-incubation; values shown indicate means ± SEMs of three independent experiments.

Figure S3. Neutralization activities of mAbs to B.1.617 variants. Related to Figure 3.
Data show the ID_{50} ratio of each variant, compared with the D614G reference strain. Dotted line indicates fourfold change.

Figure S4. Neutralization inhibition rates of mAbs to B.1.617 variants. Related to Figure 3.
Data represent the mean values of three repeat experiments.

Figure S5. Expression levels of various mammalian ACE2 orthologs on surfaces of transfected HEK293T cells. Related to Figure 2B.
Cell surface expression levels of FLAG-tagged ACE2 orthologs were assessed by flow cytometry. PE-A+ value in upper right corner represents the proportion of ACE2-expressing cells.

Figure S6. Expression levels of spike proteins of different variants on surfaces of transfected 293T cells. Related to Figure 2E and 2F.
Cell surface expression levels of spike proteins were assessed by flow cytometry. FITC-A+ value in upper right corner represents the proportion of spike-expressing cells.

Figures

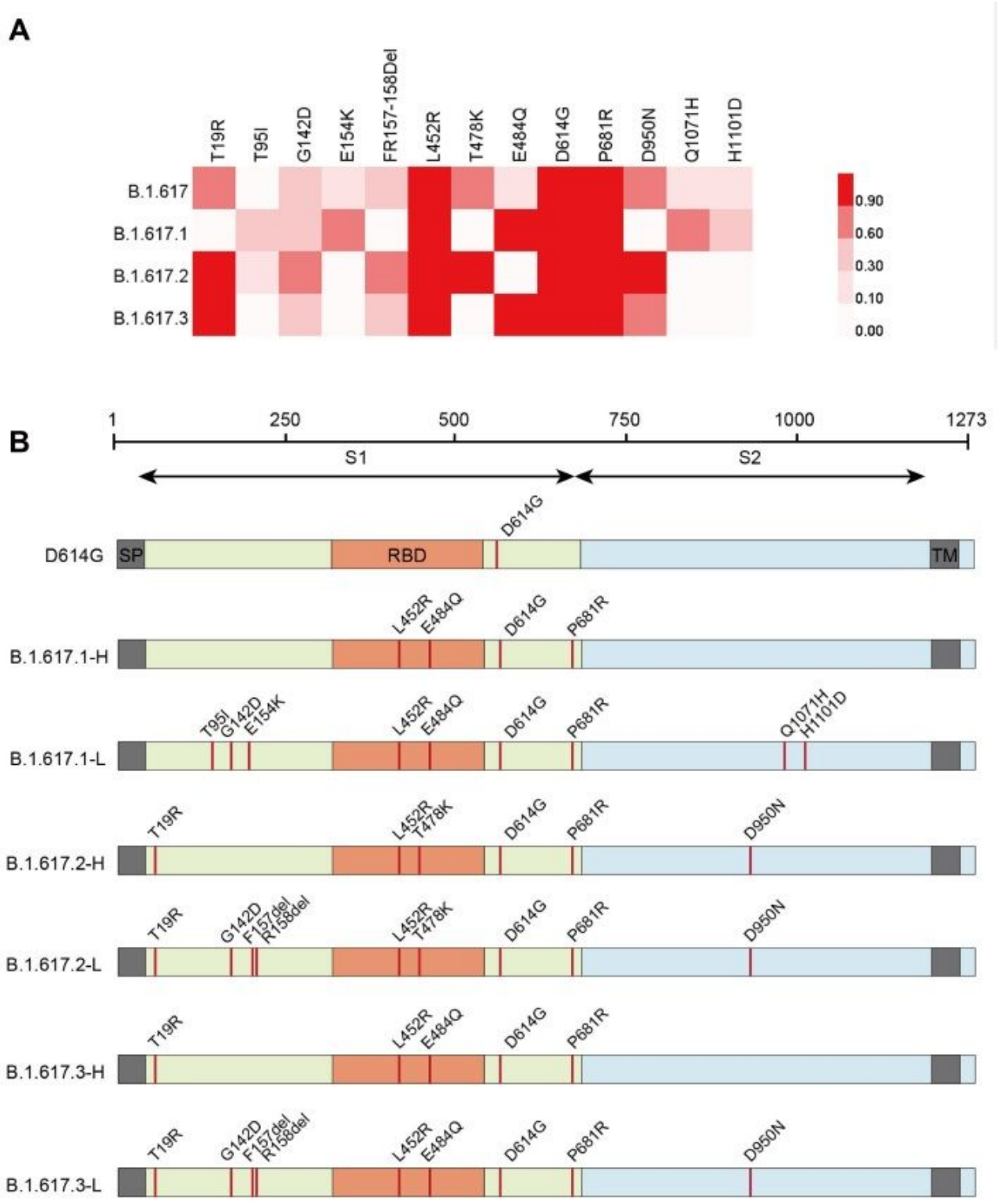

Figure 1

Analysis of mutations in B.1.617 variants. A.Mutation sites with frequencies of >30% in at least one B.1.617 sub-lineage were tracked using an outbreak website. The heatmap shows the proportions of

sequences with each mutation among all sub-lineage sequences. B. Diagrammatic sketch of B.1.617 variants that were constructed as pseudotyped viruses and analyzed in this study.

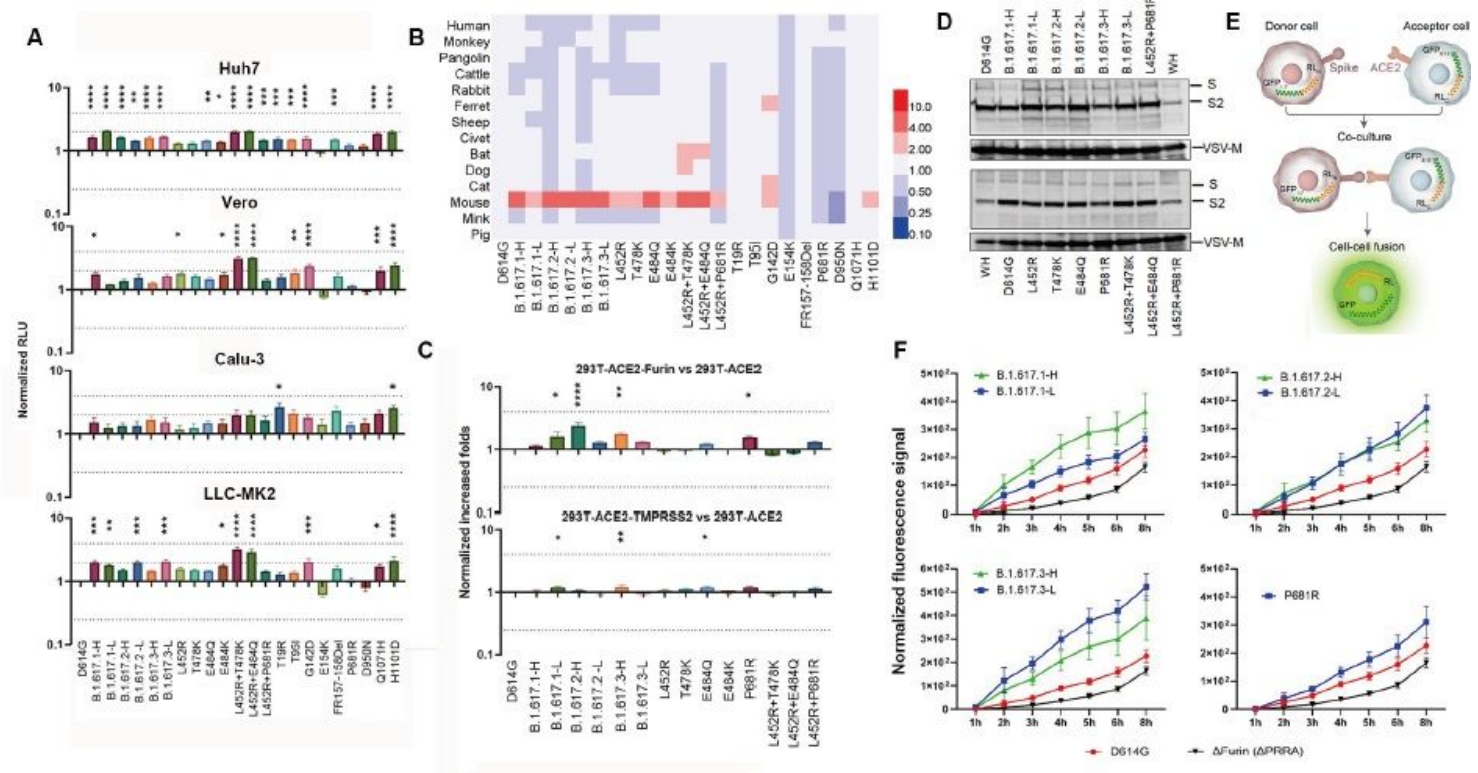

Figure 2

Analysis of B.1.617 infectivity, proteolytic activity, and cell–cell fusion A. Normalized chemiluminescence signals (in RLUs) of target cells were calculated compared with the D614G reference strain. Data represent the results of four replicate experiments. Dotted lines indicate twofold and fourfold change. B. Equal amounts of ACE2-overexpression plasmids from different species were transfected into 293T cells. Ratios of infectivity compared with the D614G reference strain were shown. Data representing the results of four replicate experiments are shown in heatmap format. Red represents increased infectivity and blue represents decreased infectivity. C. Proteolytic enzymes furin and TMPRSS2 were separately overexpressed in 293T-hACE2 cells. Data shown indicate relative infectivity changes because of enzyme overexpression. Relative RLUs were compared with or without the indicated enzyme first, then compared with the D614G reference strain. Results were obtained from four independent experiments. Dashed lines indicate the threshold of fourfold difference. D. B.1.617 and reference pseudotyped viruses were centrifuged in sucrose buffer, then resuspended in PBS for SDS-PAGE. Western blotting was performed with mouse anti-S2 polyclonal antibodies. VSV-M was used as an internal control. Representative results of three replicate experiments are shown. E. Diagrammatic sketch of dual reporter cell–cell fusion system. 293T cells were used as donor cells. F. Time course curve of cell–cell fusion. Fluorescence signals of GFP were normalized to the signal of the D614G reference strain after 1 hour of co-incubation; values shown indicate means ± SEMs. Representative results of three independent experiments are shown.

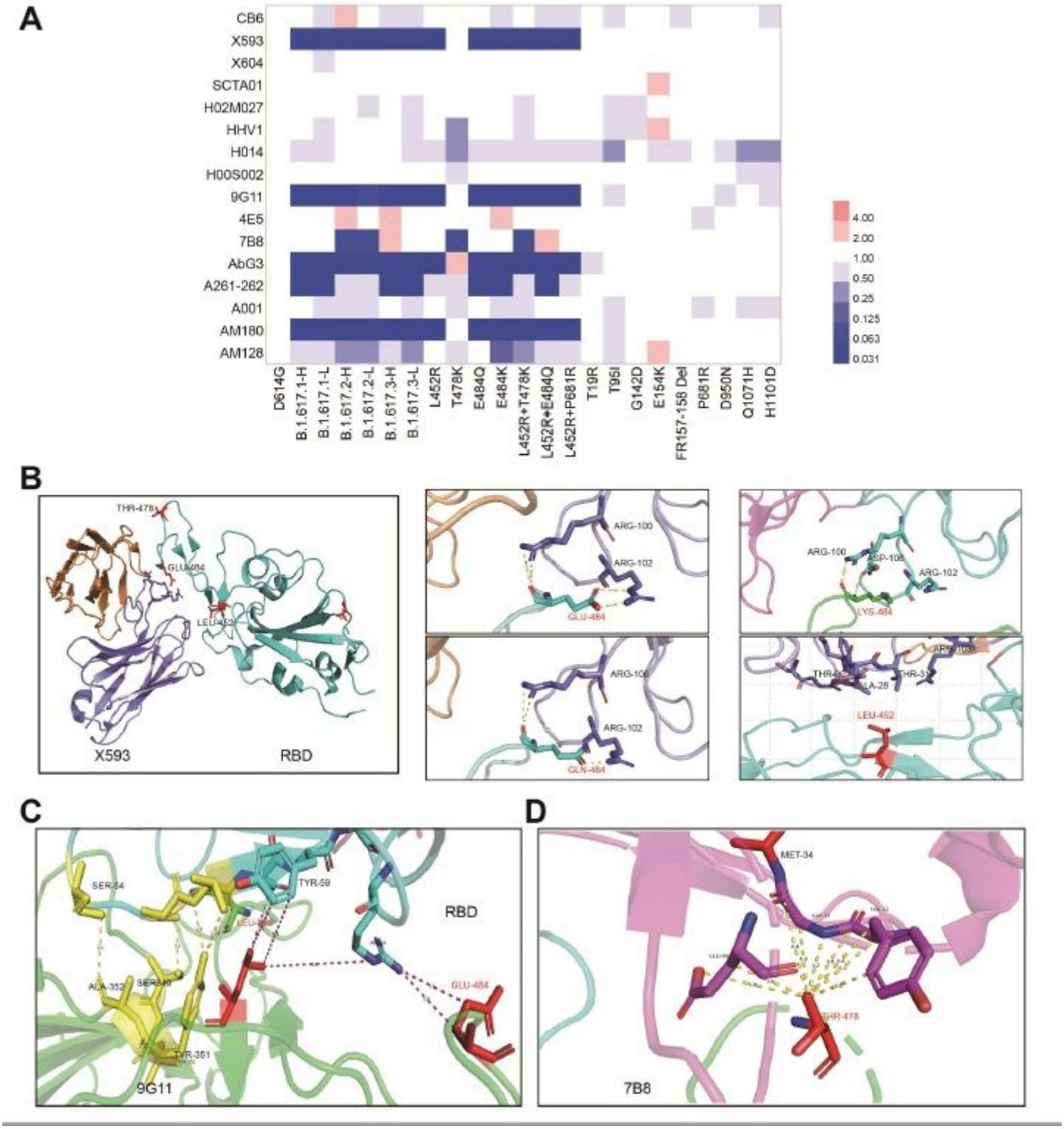

Figure 3

Neutralization activities and structural analyses of mAbs against B.1.617 variants and single point mutations. A. Data show the neutralization ID50 ratio of each variant, compared with the D614G reference strain. Red represents increased neutralization capacity and blue represents decreased neutralization capacity. B. Structural modelling of the L452R, T478K, and E484Q mutations, based on 7chh for X593, RBD-7B8 for 7B8, RBD-Ab5 for 9G11, and 7c01 for CB6.

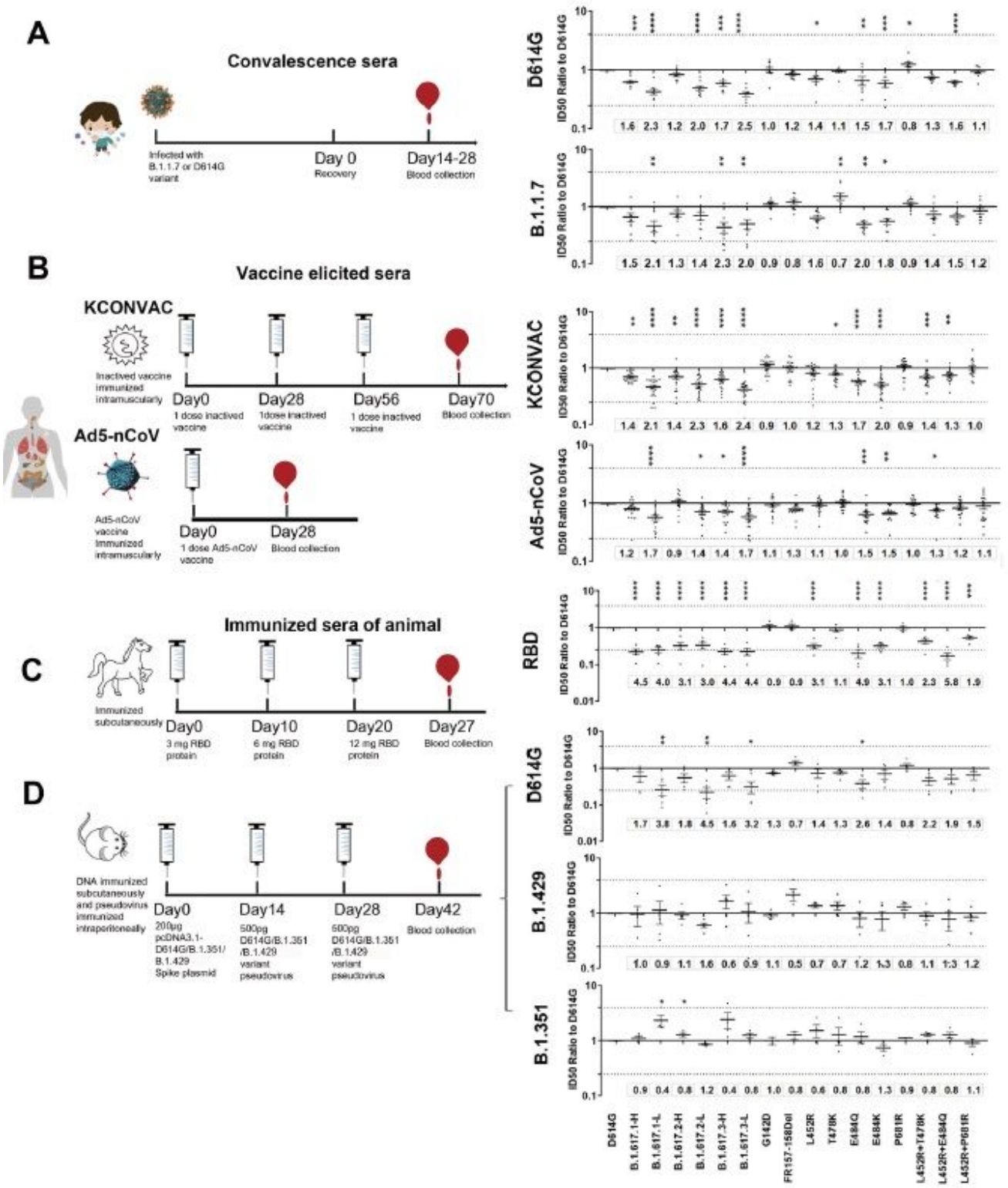

Figure 4

Neutralization activities of convalescent sera and immunized sera. Normalized ID50 ratios compared to D614G reference strain are shown. Means ± SEMs are shown for each variant. Dashed lines indicate the threshold of fourfold difference. Reduced differences (compared with the D614G reference strain) are labeled at the bottom of each plot. All experiments were repeated 2–4 times, depending on sample availability. A. Neutralization activities of convalescent sera. B. Neutralization activities of vaccine-

immunized sera. C. Neutralization activities of RBD protein-immunized horse sera. D. Neutralization activities of sera from full-length spike DNA-immunized and pseudotyped virus-immunized mice. Immunization procedures are shown in the left panel.

Supplementary Files

This is a list of supplementary files associated with this preprint. Click to download.

- FigS1.pdf
- FigS2.pdf
- FigS3.pdf
- FigS4.pdf
- FigS5.pdf
- FigS6.pdf
- SupplementaryTable.xlsx